

Evidence for "Alpha-Particle" Clusters in Several Nuclei from the $(\alpha, 2\alpha)$ Reaction at 0.91 BeV*

G. IGO, L. F. HANSEN,† AND T. J. GOODING‡

Lawrence Radiation Laboratory, University of California, Berkeley, California

(Received 28 February 1963)

We have investigated the "alpha-particle" cluster density in the region, $\rho < (1/20)\rho_0$, utilizing the $(\alpha, 2\alpha)$ reaction at 0.915 BeV. The results are consistent with complete clustering of all nucleons in the density region $\rho < (1/20)\rho_0$. In this region nucleons are less affected by the Pauli principle. When nucleons emerge from the inner region ($\rho = \rho_0$) they give the nucleus extra stability by clustering to form "alpha-particle" satellites. These structures may have a short lifetime and be constantly forming and redissolving. The alpha-particle nonelastic mean free path in nuclear matter of density $(1/20)\rho_0$ is very short (12F) and almost independent of energy as determined from elastic scattering and total-reaction cross-section measurements for alpha particles. As a consequence the reaction volume in heavy nuclei is known to be that part of the pole caps where $\rho < (1/20)\rho_0$, and the $(\alpha, 2\alpha)$ reaction is very specifically probing this layer. Coincident events were observed from a series of heavy target elements in which two emergent alpha particles were identified in which the sum of their energies was equal to 0.915 BeV. The energy of the individual alpha particle and the angular correlation between them were found to correspond to the free, two-body collision kinematics for equal mass particles. The numbers of such events were consistent with complete clustering of all nucleons in the density region $\rho < (1/20)\rho_0$.

INTRODUCTION

IN the outer fringes of heavy nuclei, nucleons tend to be less affected by the Pauli principle than in the central part of the nucleus. When nucleons emerge from the core of the nucleus, they give the nucleus extra stability by clustering together to make an "alpha particle." The lifetime may be short so that the "alpha-particle" satellites would constantly form and redissolve back into the nuclear core. A direct method, the $(\alpha, 2\alpha)$ reaction at 0.915 ± 0.005 BeV, has been used to detect the presence of "alpha-particle" clusters. By this means we have investigated the outer layers of heavy nuclei where the nucleon density ρ is less than 1/20th of the central nucleon density ρ_0 .

If an alpha-particle projectile collides with an "alpha-particle" cluster, a quasielastic collision may occur. The angle between the resulting two relativistic alpha particles will be about 87.5° and the energies will be specified by the angle of scattering if the binding energy of the "alpha-particle" clusters in nuclei is close to zero. Furthermore, the sum of the energies will add up to 0.91 BeV.

It is important to emphasize that the three conditions listed above will uniquely determine that a quasielastic collision between the incident alpha particle and an "alpha-particle" cluster took place. The experimental method used in this work to identify quasielastic events involved the following measurements. One counter telescope angle has been fixed at 22° . It is then found that a peak correlation counting rate is obtained when the other counter telescope is passed through 67.5° (where the sum of the two angles is 87.5°). The width of

the peak reflects the small momentum components of the "alpha-particle" cluster. Events are examined where the energy carried off by the alpha particles is equal to that brought in by the incident alpha particle. The energy of the alpha particles scattered into the counter telescope at 22° is examined for an event in the above-defined correlation peak. It is then found that this alpha particle carries off about 0.75 BeV. This last observation completes the specifications that the collision was between two alpha particles. If, for instance, a quasielastic collision occurred between the incident alpha particle and a "di-nucleon" cluster, the energy of the alpha particle would be about 0.5 BeV (instead of the observed 0.75 BeV). The di-nucleon would incidentally have to pick up two more nucleons on the way out of the nucleus to satisfy the requirement of being an $(\alpha, 2\alpha)$ event. If the quasielastic collision were between the incident alpha particle and a nucleon, the possibility of scattering the incident alpha particle at 22° would be kinematically forbidden. It has to be stated that a collision between a projectile and a nucleon with a very high momentum followed by a pickup process can always be found which will reproduce the three $(\alpha, 2\alpha)$ kinematical conditions specified above. However, it would also require that other equally high momentum components did not contribute in order that the correlation function we see be observed.

The fact that the refractive effects of the Coulomb force field and the nuclear force field are negligible at 0.91 BeV suggests that the interpretation of the conclusions may be simple. On the other hand, it should be noted that since the over-all resolution of this method of detection is 5.5%, many states in the residual nucleus may enter into the reaction.

There already exists some evidence from at least four sources for clustering in the surface layers of heavy nuclei. These are (1) the small magnitude (10^{-8}) of the ratio of theoretical and experimental values for the re-

* Work done under the auspices of the U. S. Atomic Energy Commission.

† Permanent address: Lawrence Radiation Laboratory, Livermore, California.

‡ Permanent address: Space Sciences Laboratory, General Dynamics/Aeronautics, San Diego, California.

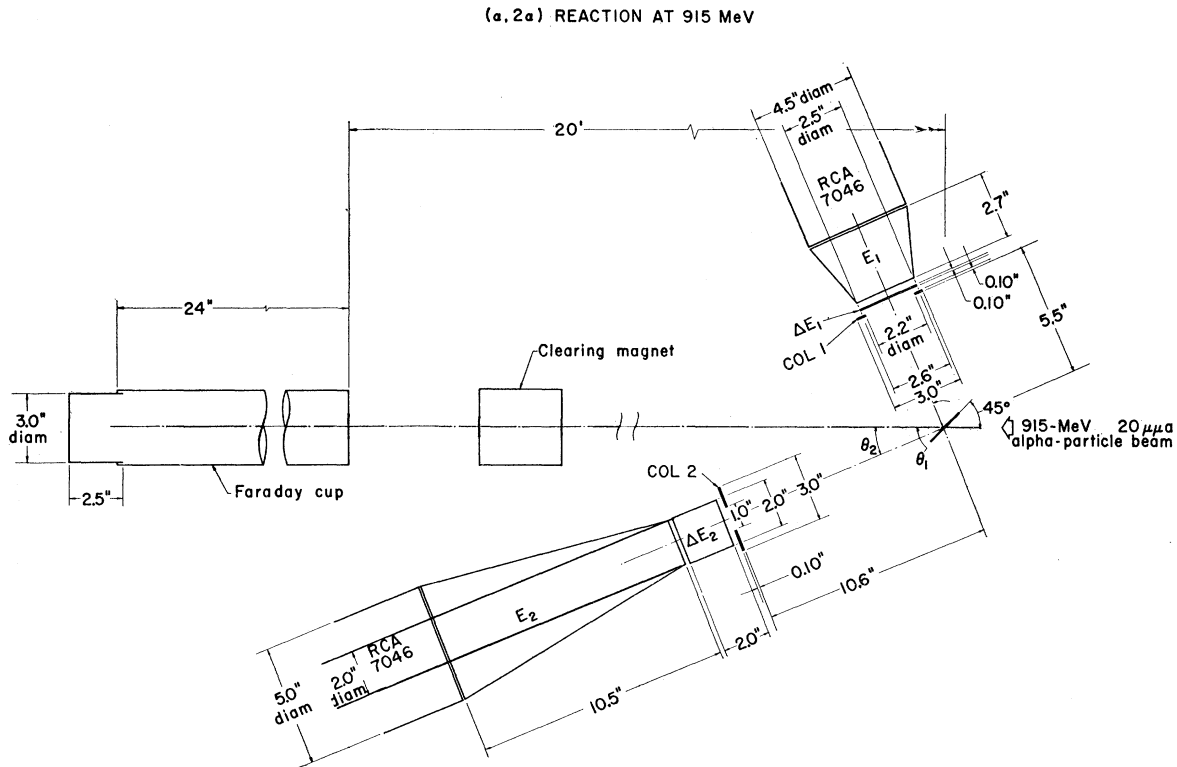


FIG. 1. Schematic diagram of the apparatus used for detecting an $(\alpha, 2\alpha)$ reaction at 0.91 BeV.

duced widths $(\theta^2)_{\text{theory}}/(\theta^2)_{\text{expt}}$ for alpha decay¹⁻³; (2) the energy spectrum of Σ hyperons produced in K^- -induced stars in emulsion nuclei⁴; (3) the energy dependence of the (p, α) reaction in the several hundred MeV range⁵; and (4) the properties of the (p, α) reaction at 30 MeV.⁶

The differential cross-section measurements of the present experiment suggest the presence of alpha particle clustering in the outer fringes of heavy-nuclei matter distributions. In addition to these measurements on Pb, Bi, and U, the quasielastic differential cross section $d\sigma/d\Omega$ is presented for three $4-n$ nuclei ($n=3, 7$, and 10), and for copper and aluminum.

The experimental method used in the present work is described in Sec. II. The experimental procedure is described in Sec. III. In Sec. IV, the experimental results and the sources of error are presented. In Sec. V, a discussion of the experimental results obtained in this experiment is made, and a comparison is made with the above-mentioned experimental information.

¹ J. O. Rasmussen, Phys. Rev. **113**, 1593 (1959).

² K. Harada (unpublished).

³ O. de Oliveira, J. Osada, N. Martins, and T. Miyazima, Nuovo Cimento **20**, 845 (1961).

⁴ D. H. Wilkinson, in *Proceedings of the Rutherford Jubilee International Conference, 1961*, edited by J. E. Birks (Heywood and Company Ltd., Manchester, 1962), p. 359.

⁵ V. I. Ostroumov and R. A. Filov, Zh. Eksperim. i Teor. Fiz. **34**, 643 (1959) [translation: Soviet Phys.—JETP **10**, 459 (1960)].

⁶ P. E. Hodgson, Nucl. Phys. **8**, 1 (1958).

II. EXPERIMENTAL METHOD

A. Counters

Figure 1 shows a schematic diagram of the apparatus used for detecting an $(\alpha, 2\alpha)$ event. The counter telescope to detect the lower energy alpha particle at an angle θ_1 consists of three plastic scintillators. A collimator counter, COL 1, which is 0.10 in. thick and 3 in. square with a 2.25-in.-diameter hole in the center is placed at a distance of 5.5 in. from the target for most of these measurements. The COL 1 counter is followed at a distance of 1/8 in. by a 0.10-in.-thick plastic scintillator ΔE_1 , 2½ in. by 3½ in. in areal size. A 90-MeV alpha particle produced at the center of the target will just stop in this counter. The ΔE_1 counter acts as a passing counter for higher energy alpha particles and will measure the differential energy loss integrated over an energy range determined by the energy E_T at the center of the target. The stopping counter E_1 is placed 1/8 in. behind ΔE_1 and is thick enough to stop 400-MeV alpha particles produced in the target. It is a plastic scintillator of a conical shape with 2-in. and 4.5-in.-diameter faces and a height of 3 in.

At θ_2 a similar counter is placed to detect the forward-scattered, higher energy alpha particle. It is similar (see Fig. 1) to the configuration at θ_1 with the following exceptions. The collimator counter, COL 2, was placed at a distance of 10.6 in. from the target and has a 1-in.-

diameter hole; plastic scintillator ΔE_2 is a 2-in. cube; and E_2 has 1.5-in. and 4.5-in.-diameter faces and a length of 10 in. This telescope is capable of stopping alpha particles with $E_T=950$ MeV.

The collimator counters, COL 1, COL 2, are large enough to anticoincidence out events in which the ΔE or E counters are struck by spurious products outside the collimated area from the target. The ΔE counters are sufficiently thick so that the pulse-height resolution is good enough to be able to differentiate against energetic He^3 reaction products as well as singly charged products entering the counter telescope. Two considerations determine their thicknesses. The first, the number of photoelectrons produced in the photomultipliers, must be large enough to reduce the statistical uncertainty to the required value; and second, the energy loss must be large enough so that the Landau-Symon energy-loss fluctuations⁷ are reduced to a level where they will not limit the resolution. Data on the response of plastic scintillators to singly and doubly charged particles available in the literature⁸ was used to calculate the response to these ions. The statistical uncertainty associated with photoelectron multiplicities was calculated using a conservative value of 10-keV/photoelectron. The Landau-Symon distribution was folded with the photoelectron statistical distribution to determine the energy spread. The energy spread was subsequently converted to spread in pulse-height distribution for each

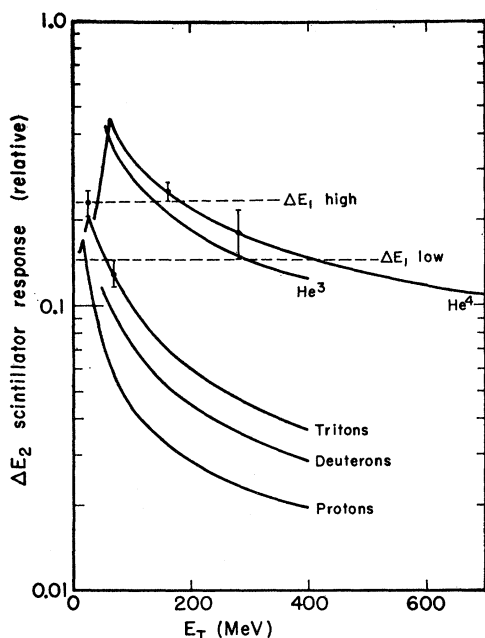


FIG. 2. The response of the ΔE_1 counter to high-energy charged particles.

⁷ B. Rossi, *High-Energy Particles* (Prentice-Hall, Inc., Englewood Cliffs, New Jersey, 1952), p. 31.

⁸ T. J. Gooding and H. G. Pugh, *Nucl. Instr. Methods* 7, 189 (1960).

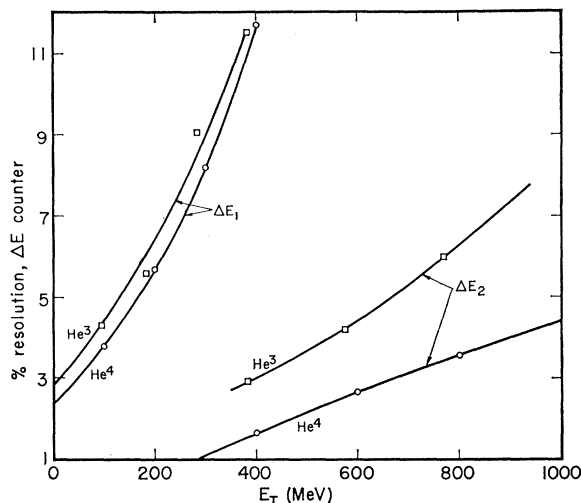


FIG. 3. The energy resolution of the ΔE_1 counter and the ΔE_2 counters.

ion. The thicknesses of the ΔE counters were in this way determined in order to permit separation of He^4 ions from He^3 and singly charged particles in the range 60–400 MeV at θ_2 and 400–950 MeV at θ_1 . Figures 2 and 3 show the response of the ΔE_2 counters and the resolution of ΔE_1 and ΔE_2 counters, respectively.

The E_1 and E_2 scintillators were made conical in shape to reduce to a minimum the volume of the plastic scintillator and still contain the divergent paths of the alpha particles associated with the size of the subtended solid angle. The counter dimensions were increased so that deviations from straight-line trajectories due to multiple-Coulomb scattering would not cause a loss of energy outside the sensitive volume of the plastic scintillator. Finally, the dimensions were further increased to allow for possible misalignment in the counter positions. Figure 4 shows the calculated response of the counter telescope to He^3 ions, He^4 ions, and singly charged ions as a function of energy.

The pulse-height resolution as a function of position in the counters was checked by moving a collimated beta source along the surfaces of the plastic scintillators. As a check on the beta-ray results, the counters were placed in a collimated 40-MeV alpha-particle beam and the pulse height checked as a function of position. It was possible to check various geometrical shapes. The shapes described above were found to give less than 1% variation in pulse height at any point on the surface of the plastic scintillator. Unfortunately, it was not possible to explore the pulse-height response beyond the range of 40-MeV alpha particles and of the beta particles particularly in the E counter. However, it is generally true that the pulse-height response varies most rapidly at the edges of a plastic scintillator.

The counters were subsequently put in the direct beam of 0.91-BeV alpha particles, 1.13-BeV He^3 ions,

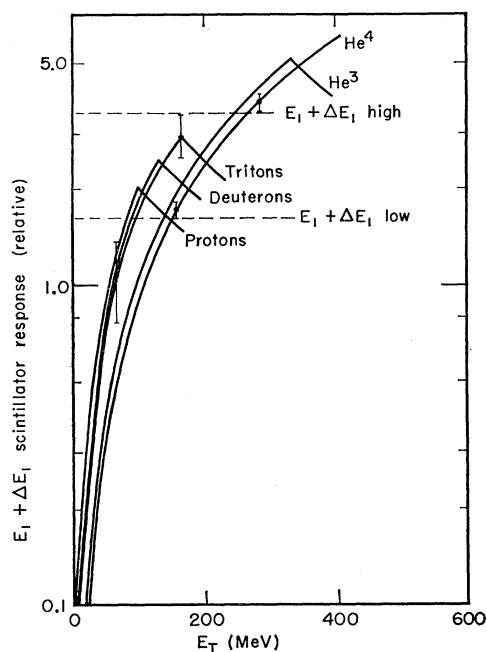


FIG. 4. The calculated $E_1 + \Delta E_1$ response to He^3 and He^4 ions and to singly charged particles as a function of energy.

and 0.70-BeV protons to check the response calculations, and some of the experimental points are also shown in Figs. 3 and 5. It has been found earlier⁹ that the pulse-height output from the counters dropped when the full beam was turned on. In order to correctly compensate for this effect, Ar-2 light flashers¹⁰ were mounted on all counters. The light flasher intensity was stable within about 1% over the 6-weeks running period.

B. Beam Handling

The 0.915 ± 0.005 -BeV alpha-particle beam from the 184-in. Berkeley synchrocyclotron was spread-out in time by an auxiliary dee. The beam can be distributed reasonably uniformly over a 12-msec time interval out of the approximately 17-msec period of the synchrocyclotron cycle. The extracted beam was collimated to a size of $1/4$ in. \times $1/4$ in. The collimated beam passed through a bending magnet to remove slit-scattered particles produced in the collimators and through a quadrupole lens which produces an image at the center of the scattering chamber with no further collimation. It was, however, necessary to place a foil in the beam pipe about 15 ft from the target to protect the cyclotron vacuum system in case the scattering chamber vacuum system failed. Interactions produced in this foil were far enough away so that solid angle considerations ruled them out as contributing to the counting rate.

⁹ T. J. Gooding and G. Igo, Phys. Rev. Letters 7, 29 (1961).

¹⁰ Q. A. Kerns and R. Tusting, Lawrence Radiation Laboratory (private communication).

The more important function of this foil from the viewpoint of the experiment was to remove the possibility of helium gas from the ion source adsorbing on the targets to give spurious results. Two comments about the possibility of helium contamination should be made. It is observed that the differential cross section for carbon varies directly with the thickness of the target, as it should, if it is due to events associated with the target material and is not constant as it would be if the He^4 contaminant were responsible. The amount of adsorbed helium necessary to explain the results reported in this paper would be approximately 0.1, 0.008, 0.10, and 0.002 moles of He/cm^2 on the carbon, calcium, copper, and lead target surfaces. There, a monolayer would be of the order of 10^{-7} moles of He/cm^2 so the effect of helium contamination is negligible.

After passing through the target, the beam passes through a flux of 2.5 kOe-cm to sweep away delta rays produced in the target, and at a distance of 20 ft from the target, behind a 10-ft-thick, concrete shielding wall, the beam is collected in a Faraday cup designed to minimize the loss of backscattered secondary electrons and of sufficient thickness to stop the helium beam ions (see Fig. 1). The beam size with the target in place at the Faraday cup position (about 1.5 in. diam) was small compared with the Faraday cup opening, and the cup

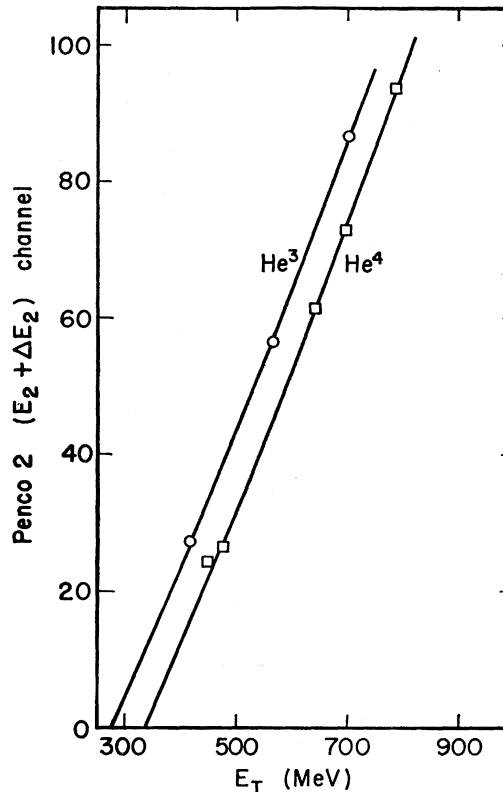


FIG. 5. The $E_2 + \Delta E_2$ response as a function of the energy for doubly charged particles in plastic scintillator.

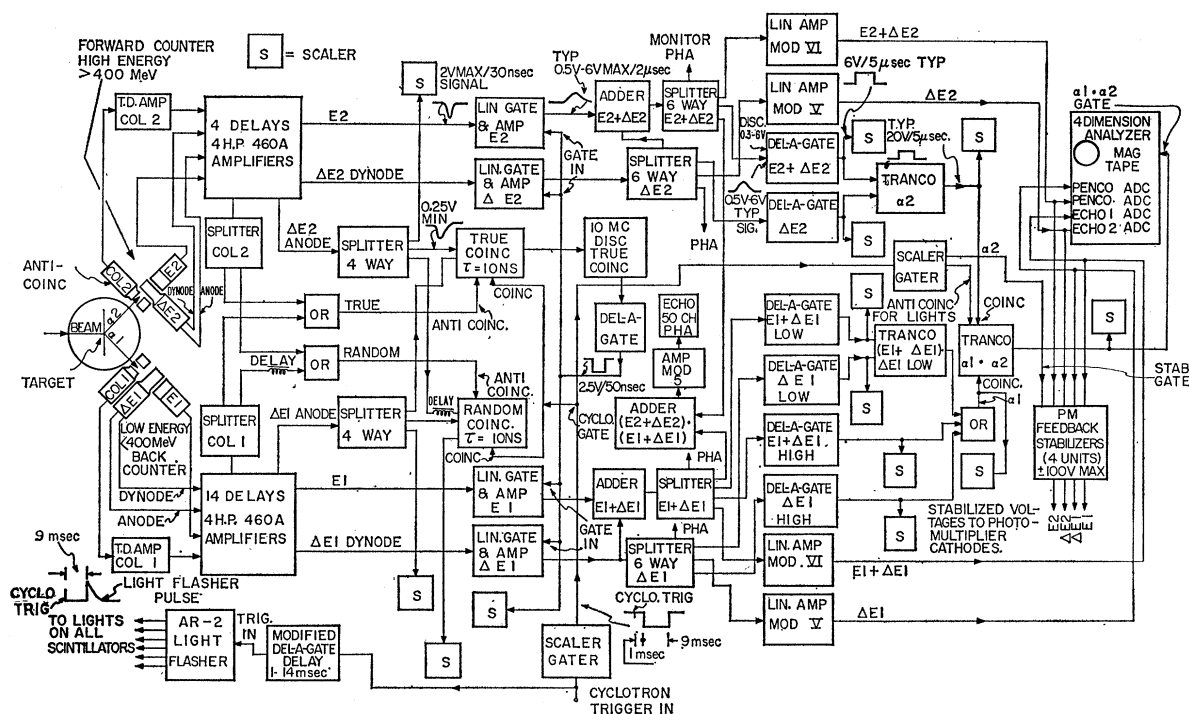


FIG. 6. Schematic diagram of the data handling system.

was well aligned on the beam. In the previous work,⁹ the beam had been monitored by an ionization chamber. It was discovered by comparison with the Faraday cup readings that the ionization chamber calibration had been incorrect. Consequently, the absolute cross sections reported in that paper are incorrect and the correct values are summarized below for helium. It should be noted that the quantity of main interest in that work as well as this is the ratio of cross sections, not the absolute value.

TABLE I. The experimental quantities for the $(\alpha, 2\alpha)$ experiment. The quantity N_T is the number of target atoms/cm²; Q , the charge collected in the Faraday cup; P , the events obtained when $\theta_1 + \theta_2 = 87.5^\circ$. Other quantities are defined in the text. In quoting N_T the target orientation (45° with respect to the beam line) is taken into account.

Element	Target thickness (mg/cm ²)	N_T (10 ²² cm ⁻²)	Q (m μ C)	P	$[\frac{d\sigma}{d\Omega}]/[\frac{d\sigma}{d\Omega}]_{He}$
He	(3080 cm STP)	10.3	211	413	
C	263	1.86	124	119	5.3 ± 1.7
Al	433	1.37	187	30	3.9 ± 1.2^a
Si	546	1.66	120	45	1.2 ± 0.5
Ca	446	1.19	236	16	2.1 ± 0.9
Cu	544	0.91	227	28	0.75 ± 0.35
Pb	752	0.388	1192	16	1.8 ± 1.3
Bi	628	0.322	398	3	0.45 ± 0.20
U	1402	0.628	946	8	0.4 ± 0.3
					0.17 ± 0.09

^a Weighted average using also the data from reference 9 as described in text.

C. Targets

Table I lists the thicknesses of the targets used in the experiment. The solid targets were oriented 45° with respect to the beam line (see Fig. 1). The thickness was adjusted so 100-MeV alpha particles produced in the target would be capable of passing through the ΔE_1 counter and registering in the E_1 counter. The helium target was a 1.090-in.-o.d. steel sphere with 0.030-in. walls. In use it was cooled to liquid-nitrogen temperatures and filled with helium gas to a nominal pressure of 5000 lb/in². The counter telescope at θ_1 , subtended a solid angle sufficiently large to intercept all scattered alpha particles produced in elastic scattering events where the partner alpha particle entered the counter telescope at θ_2 . Consequently, the differential cross section at θ_2 for elastic scattering of 0.91-BeV alpha particles from helium $d\sigma/d\Omega_{He}$ was measured directly. When a quasielastic $(\alpha, 2\alpha)$ event occurs in one of the solid targets however, the angular correlation need not be sharp, but instead, will reflect the momentum of the struck "alpha-particle" cluster. Consequently, it is necessary to measure an angular correlation function by varying the angle θ_1 . No measurements were made where θ_1 was varied out of the scattering plane, and consequently, it had to be assumed in the calculation of the differential cross section $d\sigma/d\Omega$ that the correlation function had the same shape out of the scattering plane as measured in the scattering plane.

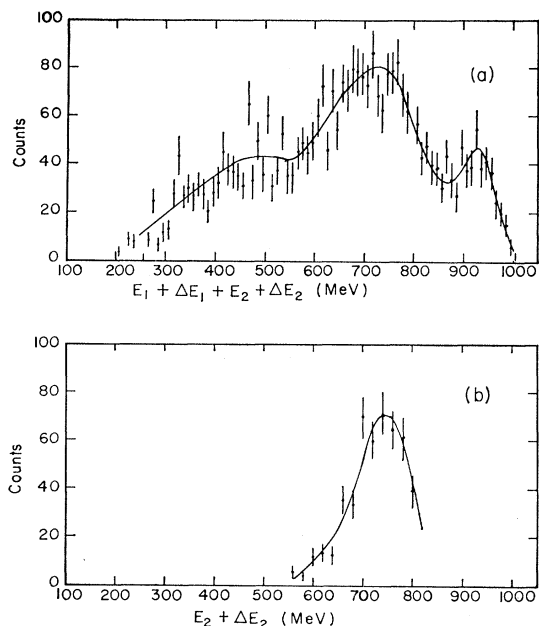


FIG. 7. (a) The energy sum spectrum at $\theta_2=26^\circ$ and $\theta_1+\theta_2=87^\circ$ for carbon. (b) The energy spectrum of the count from Fig. 7(a) in counter telescope 2 when the energy sum is greater than 850 MeV.

D. Electronics

An event was recorded when a coincidence ($\tau=10$ nsec) occurred (Fig. 2). This coincidence event was registered when the criterion

$$[(\Delta E_1)(\Delta E_2)(\overline{\text{COL}}_1)(\overline{\text{COL}}_2)]$$

was satisfied, where the bracketed quantity represents a coincidence or anticoincidence between the counters designated by the parenthesized quantities. A bar indicates an anticoincidence requirement. The collimator counters, COL_1 and COL_2 , were viewed by RCA 7264 photomultipliers. The output pulses triggered a tunnel diode discriminator¹¹ to give uniform pulse outputs 50 nsec wide which were convenient for anticoincidences. The ΔE scintillators were viewed by RCA 7264 photomultipliers. The anode output was split and fed into Wenzel coincidence circuits,¹² one for real events, and one in which ΔE_1 and COL_1 were delayed by one rf period to measure the random coincidence rate_{rand} (see Fig. 6).

In order to coordinate the timing of the electronics with the arrival of the beam in the 17-msec period associated with the 60-cycle synchrocyclotron cycle, gating circuits were fired off the synchrocyclotron rf pulse at a fixed time before the beam arrival time. These gate signals were adjusted in length and time delay to gate on

¹¹ A. E. Bjerke, Q. A. Kerns, and T. A. Nunamaker, Lawrence Radiation Laboratory, Report UCRL-9838, 1961 (unpublished).

¹² W. A. Wenzel, Lawrence Radiation Lab. Report UCRL-8000, 1957 (unpublished).

the Ar-2 light flashers¹⁰ during the beam-off part of the 17-msec period; to gate on the stabilizers to accept (Trig in, Fig. 6) the output of the linear amplifiers during the time when pulses due to light flashers arrive (Stab gate, Fig. 6); and to gate off the four-dimensional analyzer during this time period (Anticoin for lights, Fig. 6).

Light flasher pulses from the counters were able to pass through all the electronics up to and including the linear amplifiers. The output of the amplifiers was fed to the photomultiplier feed-back stabilizers (PM feed-back stabilizer, Fig. 6) which adjusted the voltages to keep the light-flash pulse heights constant.

A fourth gate ("Cyclo gate," Fig. 6) was fed into the fast coincidence circuits. It was adjusted in length and time in order to cut out the initial spike of beam sometime associated with the spread-out beam. As stated above, the spread-out beam could be made quite uniform in intensity by proper adjustment of the synchrocyclotron. However, sudden shifts were observed in the synchrocyclotron performance which resulted in a large beam spike momentarily. The spike had to be cut out because it greatly increased the number of random events. This led to an additional complication, since in this way the beam in the spike, which could be appreciable, should be discounted from the integrated beam reading from the Faraday cup. This was accomplished by scaling (S , Fig. 6) the "True Coinc" coincidences events and the "Random Coinc" coincidences as shown in Fig. 6, and by simultaneously scaling these same quantities without inserting the "Cyclo gate" pulse (not shown in Fig. 6). Utilizing the four quantities obtained in this fashion, the integrated beam readings were appropriately corrected. The correction was important since it varied between zero and 17%.

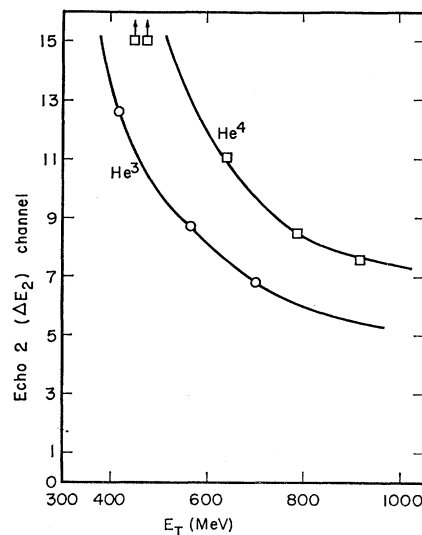


FIG. 8. The pulse-height response of the ΔE_2 counter to doubly charged particles.

When a $[(\Delta E_1)(\Delta E_2)(\overline{\text{COL}}_1)(\overline{\text{COL}}_2)]$ event occurred, the output of the ‘‘True coin’’ coincidence circuit, after amplification and delay, was fed into a discriminator. The discriminator circuit¹³ (Del-a-gate, Fig. 6) produces a uniform height, variable width, variable delay pulse. The output is used to gate on four linear gates (Lin gate and Amp, Fig. 6). Linear dynode and anode pulses from the ΔE photomultipliers and the E RCA 7046 photomultipliers, respectively, falling within the gate pulse time (50 nsec for E pulses and 20 nsec for ΔE pulses) were passed through, amplified, and stretched so that they could be handled by conventional microsecond electronic techniques. In this way, spurious background pulses were removed, and conventional microsecond electronics could be used throughout the remainder of the data analysis system.

The E_1 and ΔE_1 outputs and E_2 and ΔE_2 outputs of the linear gates were subsequently added (Adder, Fig. 6) and the pulse heights $E_1 + \Delta E_1$, ΔE_1 , $E_2 + \Delta E_2$, and ΔE_2 were then used for data analysis after being split (Splitter 6 way, Fig. 6). One or two splitter outputs are fed into discriminators (Del-a-gates $E_2 + \Delta E_2$, ΔE_2 , $E_1 + \Delta E_1$ LOW, ΔE_1 LOW, $E_1 + \Delta E_1$ HIGH, $E_1 + \Delta E_1$ LOW) set at suitable levels to remove events involving singly charged particles at θ_1 and θ_2 from the total number of

$$[(\Delta E_1)(\Delta E_2)(\overline{\text{COL}}_1)(\overline{\text{COL}}_2)]$$

events.

The discriminator settings were rechecked, and adjusted to the proper settings wherever necessary at the beginning of each day's run. A predetermined method involving the constant height light-flasher pulses was used. Appropriate outputs were subsequently fed into coincidence units (Tranco α_2 and Tranco ($E_1 + \Delta E_1$), ΔE_1 low, Fig. 6) and into an ‘‘or’’ unit (OR, Fig. 6). The outputs (Tranco α_2 and OR, Fig. 6) are fed into coincidence (Tranco $\alpha_1 \cdot \alpha_2$, Fig. 6). The latter coincidence unit output pulses correspond to all events in which two

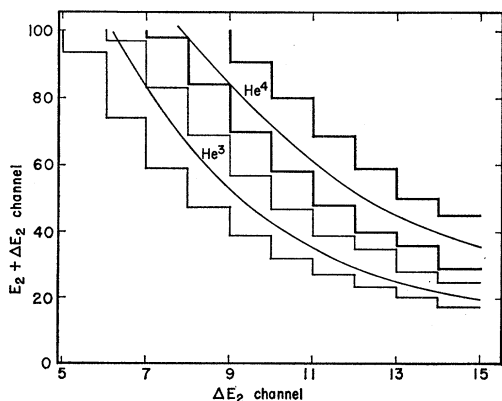


FIG. 9. The smooth curve delineates the most probable pairs of pulse heights for He^3 and He^4 ions in the counter 2 telescope. The heavy and light step functions enclose pulse-height regions corresponding to He^4 and He^3 ions, respectively.

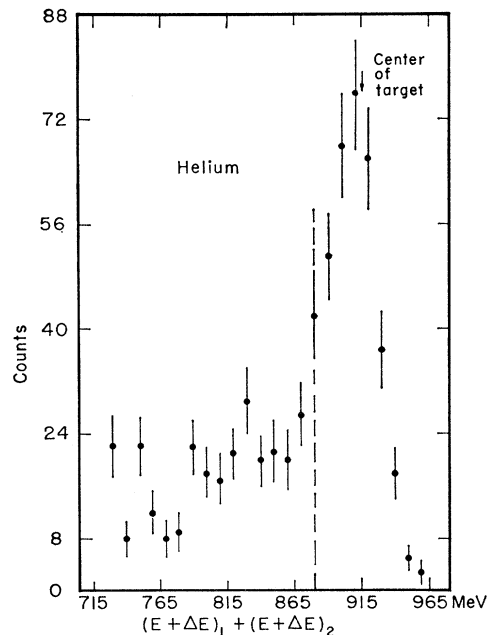


FIG. 10. The energy sum spectrum for helium for $\theta_2 = 22^\circ$ and $\theta_1 + \theta_2 = 87.5^\circ$.

doubly charged particles were recorded simultaneously at θ_1 and θ_2 . This output is used to gate on the four-dimensional analyzer. Some events involving singly charged particles also may trip this coincidence unit since the preceding separation method is not 100% effective.

The linear amplifier output pulses (Lin Amp Mod VI and Lin Amp Mod V, Fig. 6) were analyzed when a gate signal was received (Penco ADC and Echo ADC, respectively, Fig. 6) and recorded on magnetic tape in sequence. An IBM 7090 computer was used to analyze the four correlated pulse heights for each event. The events were classified into four categories. These were events where at θ_1 and θ_2 two He^4 ions, two He^3 ions, a He^3 ion and a He^4 ion, or a singly charged ion in either counter telescope was detected. Each of the first three classifications was then separately analyzed utilizing the computer. In this way (for events in the first classification, for example) it was possible to determine the energy of each alpha particle from calibration data also fed to the computer (see Sec. III), to add these energies for each event to obtain the number of events vs the total energy $E_1 + \Delta E_1 + E_2 + \Delta E_2$ of the alpha particles energy sum spectrum [see Fig. 7(a)]. The number of events at θ_1 in which the total energy $E_1 + \Delta E_1 + E_2 + \Delta E_2$ lay between certain limits vs the energy $E_1 + \Delta E_1$ of the alpha particle detected in θ_1 [see Fig. 7(b)] could also be obtained. The beam levels were always low enough so that the number of random events (Tranco $\alpha_1 \cdot \alpha_2$, Fig. 6) were negligible. In order to measure this quantity, the COL_1 , ΔE_1 dynode, ΔE_1 anode, and the E_1 photomultiplier outputs were delayed by 1 rf burst.

TABLE II. Sources and magnitudes of error in the measurement of $d\sigma/d\Omega_{He}$. The values quoted are standard deviations.

Source	Error (%)
Helium vessel pressure	± 1
Helium vessel temperature	± 3
Statistical error on P	± 5
Peak cutoff channel (see Fig. 7)	± 9
Target areal density	< 0.5
Faraday cup calibration	< 0.5
Rms standard error	± 12

III. EXPERIMENTAL PROCEDURE

A. Counter Calibrations

The light-flasher pulse heights in counters E_1 , ΔE_1 , E_2 , and ΔE_2 were first adjusted to be equal to the maximum pulse heights from events to be recorded by each counter. The photomultiplier stabilizers (see Fig. 6) were then set to monitor the corresponding light-flasher pulse height in case of gain shifts. It was found that the light-flasher output was stable over the 6-week running period to nearly 1%. For calibration purposes the COL₂, E_2 and ΔE_2 counter array was swung into the beam line (see Fig. 1). A stable, low-intensity beam of 0.91 BeV He⁴ ions or 1.135 BeV He³ ions from the synchro-cyclotron were energy degraded in copper absorbers to calibrate the E_2 and ΔE_2 counter response to these ions (see Figs. 3 and 5). As described in Sec. II, the quantities recorded by the four-dimensional analyzer are actually the sum of the two pulse heights from the E_2 and ΔE_2 counters, $E_2 + \Delta E_2$, and the pulse height from the ΔE_2 counter, ΔE_2 . At the same time the energy resolution of the counters was determined for He³ and He⁴ ions. The calibration data was used in the computer program for separating out He⁴ ion events, or alternatively He³ ion events, in the doubly charged spectrum.

B. Separation of Singly Charged Particles

To set the discriminators (Del-a-gate, Fig. 6) for separating out singly charged particles, the following procedure was adopted: Counter telescope 1 was put in the low-intensity beam. The alpha-particle energy was degraded to 278 MeV and $\Delta E_1 + E_1$ HIGH discriminator was adjusted to fire on half the events (see Fig. 4). The energy resolution of the E and ΔE counters had previously been calculated from the response curves. From this data, it was determined that a He⁴ ion with energy greater than 290 MeV would have a high probability of firing $E_1 + \Delta E_1$ HIGH and a singly charged particle of any energy (see Fig. 4), would have a low probability. Therefore, to the first approximation high-energy, doubly charged particles would fire this discriminator. A similar line of argument applies to the ΔE_1 HIGH discriminator setting when the resolution of the ΔE_1 counter (see Fig. 3) is taken into account. The He⁴ ions with energy less than 160 MeV fire this discriminator,

and singly charged particles are virtually excluded in their corresponding energy range. To distinguish He⁴ ions in the range between 160 and 290 MeV, ΔE_1 LOW and $E_1 + \Delta E_1$ LOW discriminators are adjusted so that the coincidence unit [Tranco ($E_1 + \Delta E_1$) $\cdot \Delta E_1$ LOW, Fig. 6] fed by the discriminator outputs will be fired by He⁴ ions in this energy range and singly charged particles in the corresponding energy range are virtually excluded. After the discriminators were so adjusted, the beam and the stabilizers were turned off. The linear gates¹⁴ were adjusted until the discriminators were just fired by light-flasher pulses. The corresponding ΔE and $E + \Delta E$ pulse heights were measured on an auxiliary pulse-height analyzer. Then the linear gate gains (see Fig. 6) were put back to their initial settings and the stabilizers turned on. At the beginning of each day's run, the discriminator levels were readjusted to the proper values by comparison with the appropriate light-flasher pulse height previously recorded on the auxiliary pulse-height analyzer.

C. Separation of Events Involving He³ Ions

Figures 8 and 5 show the response of the ΔE_2 scintillator and the sum response of scintillators, E_2 and ΔE_2 , as a function of energy at the center of the targets E_T . A smooth curve similar in slope to that predicted by the calculated response is fitted to the data. The smooth curves in Fig. 9 are obtained from Figs. 3 and 5. They represent the most probable pairs of pulse heights (Penco and Echo, Fig. 6) for He³ and He⁴ events in the counter 2 telescope. The separation of He³ and He⁴ events in the computer program was effected by feeding in the step function Penco pulse-height limits for each Echo channel for He³ and He⁴ ions obtained from this

TABLE III. Sources and magnitudes of error in the measurement of $[d\sigma/d\Omega]/[d\sigma/d\Omega]_{He}$. The values quoted are standard deviations. The error associated with the determination of the areal density of the solid targets was less than 0.5%.

Target	The rms error from Table II (%)	The statistical error on the number P of quasi-elastic events (%)	The uncertainty in the quasi-elastic distribution cutoff channels (%)	The uncertainty in the angular correlation function (%)	Rms error (%)
C	± 12	± 9	± 10	± 26	± 31
Al	± 12	± 18	± 27	± 26	± 43
Si	± 12	± 15	± 27	± 26	± 42
Ca	± 12	± 25	± 25	± 26	± 46
Cu	± 12	± 19	± 47	± 26	± 61
Pb	± 12	± 25	± 25	± 26	± 46
Bi	± 12	± 57	± 33	± 26	± 72
U	± 12	± 35	± 25	± 26	± 52

¹³ M. Brown, Lawrence Radiation Laboratory Report UCL-3307, 1962 (unpublished).

¹⁴ A. Barna and J. Marshall, California Institute of Technology, CTS-18, 1961 (unpublished).

graph. Since the experimental resolution was not always good enough for a complete separation, and since the interest was in He^4 ions, the step functions were adjusted to favor the mixing of some He^3 events into the He^4 spectrum rather than to lose some He^4 events. As a check on the efficacy of the entire separation system, the counters were placed in the direct proton beam behind copper degraders to show that protons were separated by the discriminator systems at all energies of interest.

The procedures of IIIB and IIIC were applied to both counter telescopes with minor variations.

As a final check on the method of particle separation, the helium sum spectrum (see Fig. 10) with particle separation was compared with the helium sum spectrum with only the separation afforded by the discriminators. The number of counts in the elastic peaks was the same in both spectra. The events involving He^3 ions were to be found in the low-energy tail of the unseparated spectrum.

D. Stability

The best measure of the stability of the detection apparatus was afforded by a comparison of the well-defined elastic peak obtained using the helium-gas target taken at various times during the 6-weeks running period. The number of counts per unit beam flux was found to be constant, and the pulse heights throughout the system were found to be satisfyingly stable. This was due primarily to the stability of the light flashers. The electronic components individually changed gains by marked amounts (for instance, the photomultiplier gains of E_2 , ΔE_1 , and E_1 changed by 50% when the 20 μA beam used in the experiment was turned on) but the gains of the complete systems were well stabilized.

IV. EXPERIMENTAL RESULTS

A. Differential Cross Section for Elastic Scattering of 0.91-BeV Alpha Particles from Helium

Figure 10 shows the energy sum spectrum for elastic scattering obtained from the helium-gas target after the background due to the steel ball had been subtracted off. The statistical error assigned to each point on the graph includes the error introduced by the subtraction. In the region of the peak the subtracted-off quantity was small. In Fig. 10 an arrow shows the energy E_T corresponding to a scattering of a 0.91-BeV alpha

TABLE IV. Sources and magnitudes of standard error in WKB calculation of $(\alpha, 2\alpha)$ reaction volume.

Source	Error (%)
Experimental error in σ_R measurements	± 22
Igo potential (reference 19)	± 5
WKB approximation method	± 10
Rms standard error	± 25

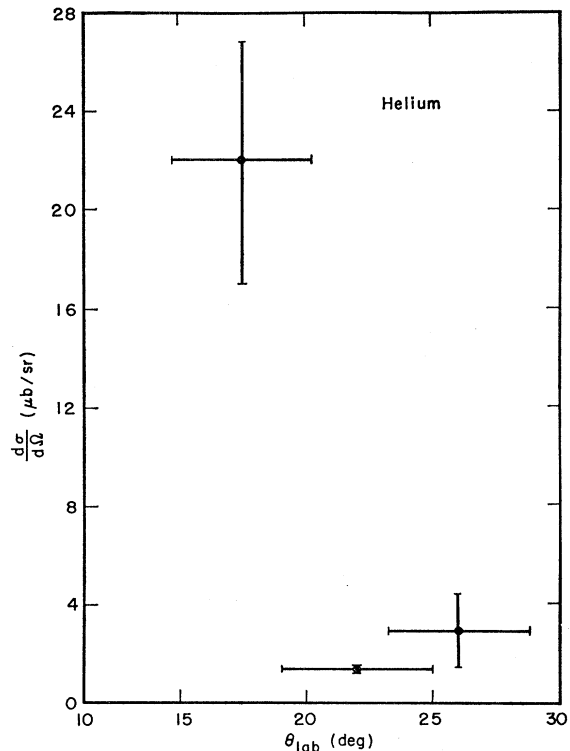


Fig. 11. The differential cross section for elastic scattering of the α particles from helium in the laboratory system.

particle from the center of the helium-gas target. The calculated spread in energies introduced by scattering at various points in the target was found to be negligibly small compared to the half-width of the peak. The observed half-width 50 MeV is, therefore, due to the over all energy resolution of the counter system. Some of the events below the peak are really elastic-scattering events since in 25% of the events, the alpha particles in the counters will suffer a nuclear reaction in the plastic scintillator which will, in general, reduce the pulse height below the proper value. Therefore, in order to obtain a correct value for the differential cross section, the number of peak counts has to be multiplied by a factor of 1.33 ± 0.16 . This factor was determined by measuring spectra with the counters in the direct beam and comparing the number of counts in the tail.

The solid angle subtended by counter 1 was large enough to collect the recoil alpha particle produced when an alpha particle was elastically scattered into the counter 2 solid angle. As mentioned above, the elastic-differential cross section $d\sigma/d\Omega_{\text{He}}$ was measured directly at $\theta_2 = 22^\circ$. It was obtained from the energy sum spectrum by summing the counts to the right of the dashed line in Fig. 10. The error ($\pm 9\%$) introduced in determining the proper cutoff for the elastic events was estimated to be of the order of the number of counts in the cut-off channel.

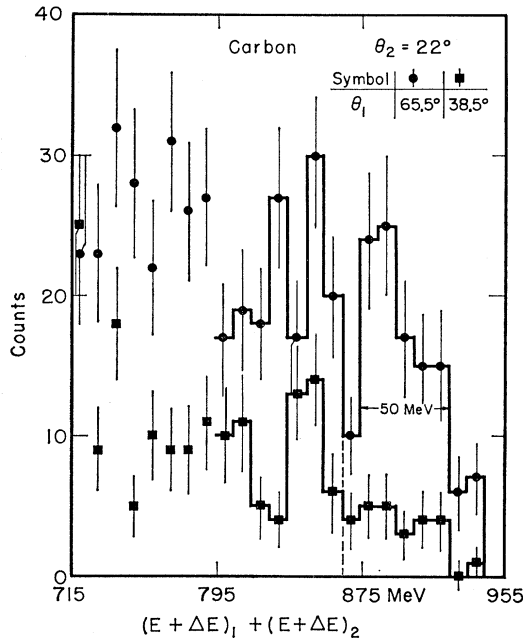


FIG. 12. The energy sum spectrum obtained from carbon at $\theta_2 = 22^\circ$ and $\theta_1 + \theta_2 = 60.5^\circ$ and 87.5° .

Other errors that enter into the calculation of the differential cross section include those due to the uncertainty in the pressure, temperature, and size of the steel ball, and in the calibration of the Faraday cup. One source of error that was judged to be small but, on the other hand, could not be evaluated, should be mentioned. The loss of charge from the stopping material (see Fig. 1) in the Faraday cup due to long-range particles produced, for example, through the (α, p) reaction could not be accounted for, since no data exists on these reactions. However, since about 25% of the particles do suffer an interaction, the connection may not be wholly negligible.

In Table I the quantities entering into the calculation of the differential cross section are shown, and in Tables II–IV the standard errors are summarized. The final value listed is the rms standard value. The differential cross section at 0.915 ± 0.005 BeV for elastic scattering of alpha particles at 22° in the lab system is $1.2 \pm 0.2 \mu\text{b}/\text{sr}$. Figure 11 shows a summary of the values obtained in this work and in reference 9. As mentioned previously in the text, the values quoted in reference 9 were based on ion chamber readings. The ion chamber readings were discovered to be too low when compared with the Faraday cup readings. The corrected values are plotted in Fig. 11.

B. $(d\sigma/d\Omega)/(d\sigma/d\Omega)_{\text{He}}$

The differential cross section $d\sigma/d\Omega$ for quasielastic scattering at 22° for C, Al, Si, Ca, Cu, Pb, Bi, and U divided by the differential cross section at 22° for elastic

scattering of alpha particles from helium, $d\sigma/d\Omega_{\text{He}}$, has been evaluated.

The energy sum spectra at $\theta_2 = 22^\circ$, $\theta_1 + \theta_2 = 87.5^\circ$ and 60.5° for C are presented in Fig. 12 normalized to the same integrated beam and the same solid angles. As was true for the helium gas target, the energy spread introduced by target thickness and the angular spread of the counters was of the order of 10 MeV whereas the energy resolution is known from the well-defined helium gas target peak to be 5.5% or 50 MeV wide (full width at half-maximum). Since no peak is defined in any of the measurements from solid targets, the energy resolution cutoff used for the helium gas target was also used for the other targets, and the error associated with the cutoff procedure was judged to be equal to the number of counts in the cutoff channel. The resulting contribution to the standard error is quoted in Table II.

As was observed in reference 9 at 17.5° and at 26° , there are more quasielastic events at the kinematical separation angle ($\theta_1 + \theta_2 = 87.5^\circ$), than at $\theta_1 + \theta_2 = 60.5^\circ$. For C, Fig. 7 shows the energy sum spectrum at $\theta_2 = 26^\circ$ and $\theta_1 + \theta_2$ equal 87° and also the energy spectrum of the counts in counter 2 where the energy sum is greater than 850 MeV. The most probable energy corresponds closely to the expected kinematical energy for a two-body collision. In summary, the experimental evidence for quasielastic scattering in carbon is as follows: (1) The coincidence counting rate is largest at $\theta_1 + \theta_2 = 87.5^\circ$; (2) The sum of the energy of the two alpha particles is equal to the initial energy minus the binding energy of alpha particles in C when energy resolution is accounted for; and (3) The energy of the individual alpha particles at θ_1 and θ_2 correspond to the free two-body kinematical values where the struck alpha-particle cluster is almost at rest. These conclusions were stated in reference 9 and have been verified by the present results.

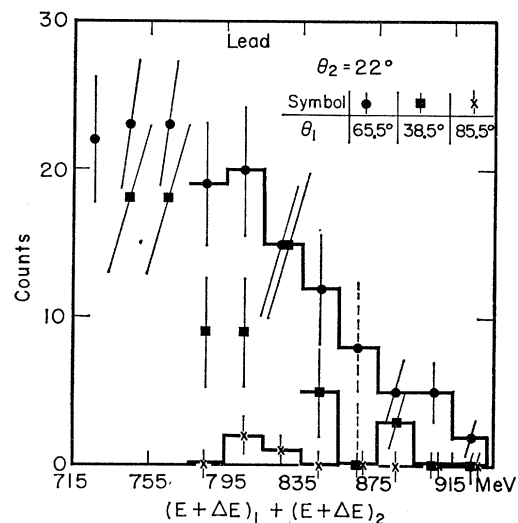


FIG. 13. The energy sum spectrum obtained from lead at $\theta_2 = 22^\circ$ and $\theta_1 + \theta_2 = 87.5^\circ$, 60.5° , and 107.5° .

The same evidence has been obtained in the $(\alpha, 2\alpha)$ sum spectra from Pb. In Fig. 13 the energy sum spectra obtained for $\theta_2 = 22^\circ$ and $\theta_1 + \theta_2 = 87.5^\circ, 60.5^\circ,$ and 107.5° is shown normalized to the same solid angle and integrated beam. The dashed line shows the cutoff used to separate the quasielastic events using the same criterion as with the helium-gas target and with C target. The energy carried separately by each alpha particle is consistent with the two-body kinematics as was the case with C. Note that the number of counts at $\theta_1 + \theta_2 = 87.5^\circ$ is larger than at either $\theta_1 + \theta_2 = 60.5^\circ$ or 105.5° . Not shown is the counter 2 spectrum for sum spectrum events in the quasielastic energy interval. A well-defined group at the proper kinematical energy is found, as was the case with C. The quasielastic $(\alpha, 2\alpha)$ process is again verified.

The same kind of evidence (Fig. 14) is found in the $(\alpha, 2\alpha)$ reaction when copper is used for the target. The $\theta_2 = 22^\circ, \theta_1 + \theta_2 = 87.5^\circ$ counting rate is higher than the $\theta_1 + \theta_2 = 60.5^\circ$ or 107.5° spectra. Measurements on Al, Si, Ca, Bi, and U at $\theta_2 = 22^\circ$ and $\theta_1 + \theta_2 = 87.5^\circ$ were also made.

In order to determine the differential cross section for the quasielastic scattering process, the shape of the $\theta_1 + \theta_2$ correlation function had to be estimated from the points measured at $\theta_1 + \theta_2 = 60.5^\circ, 87.5^\circ,$ and 105.5° . It was assumed that the correlation function was symmetric in and out of the plane and in the shape of a cone with apex at $\theta_1 + \theta_2 = 87.5^\circ$ and fitting the counting rates obtained at these three angles. In this way it was found that the multiplication factor to convert the quantity $(d^2\sigma/d\Omega_1 d\Omega_2) \Delta\Omega_1$ at $\theta_1 + \theta_2 = 87.5^\circ$ to $d\sigma/d\Omega_2$ was 2.46 ± 0.64 . The uncertainty in the conversion factor represents the upper and lower bounds on the conical volume which can fit the data. The angular correlation functions of the three targets were in agreement within the error assigned. Consequently, it was assumed that the angular correlation functions for all the targets were the same in the reduction of the data.

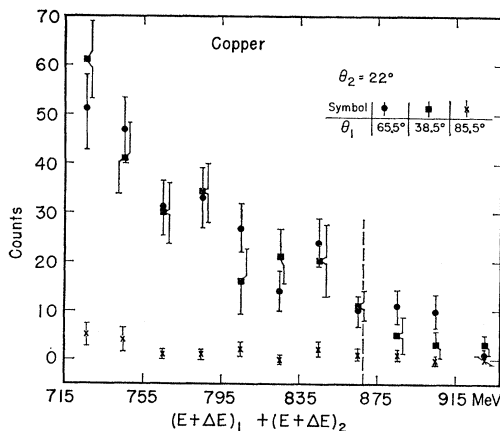


FIG. 14. The energy sum spectrum for copper obtained for $\theta_2 = 22^\circ$ and $\theta_1 + \theta_2 = 87.5^\circ, 60.5^\circ,$ and 107.5° .

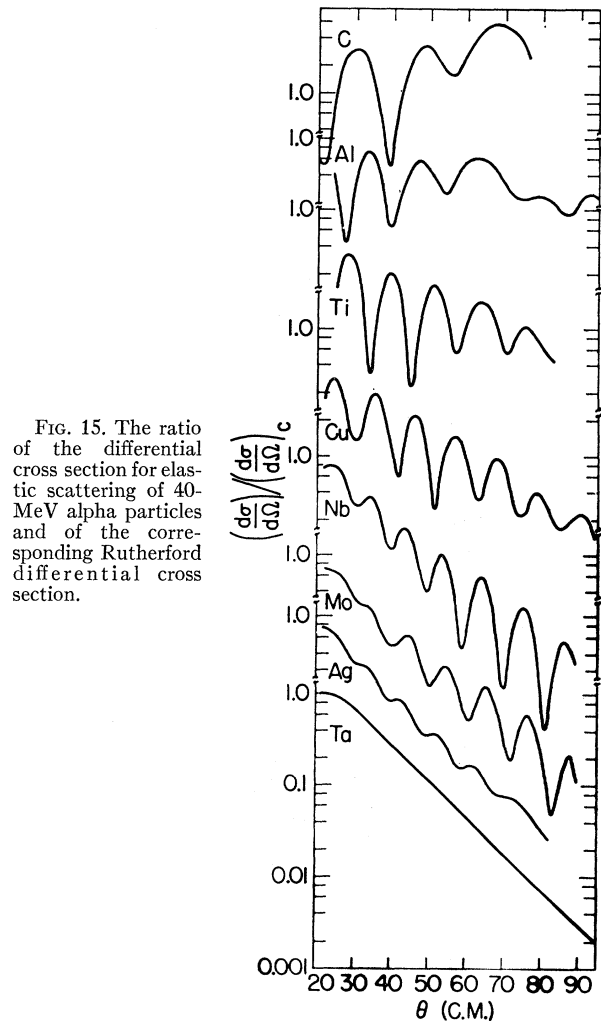


FIG. 15. The ratio of the differential cross section for elastic scattering of 40-MeV alpha particles and of the corresponding Rutherford differential cross section.

Other sources of error that enter into the final value on $(d\sigma/d\Omega)/(d\sigma/d\Omega)_{He}$ are shown in Table III. These include the statistical error on the number of counts in the quasielastic peak. The error on target areal densities was negligible compared with other sources of error. The ratio $(d\sigma/d\Omega)/(d\sigma/d\Omega)_{He}$ is listed in Table I for C, Al, Si, Ca, Cu, Pb, Bi, and U, and the errors have been compiled in Table III.

For C, three measurements for $(d\sigma/d\Omega)/(d\sigma/d\Omega)_{He}$ exist. These are 1.7 ± 0.9 at 17° and 3.9 ± 2.9 at 26° from reference 9, and 5.3 ± 1.7 from the present work. The weighted mean value for $(d\sigma/d\Omega)/(d\sigma/d\Omega)_{He} = 3.9 \pm 1.2$ for C.

V. INTERPRETATION OF RESULTS

A. Carbon

The best data available on quasielastic $(\alpha, 2\alpha)$ scattering at 0.91 BeV is for C. The value for $(d\sigma/d\Omega)/(d\sigma/d\Omega)_{He}$ of 3.9 ± 1.2 suggests that alpha clustering in carbon is nearly 100% complete. It should be pointed

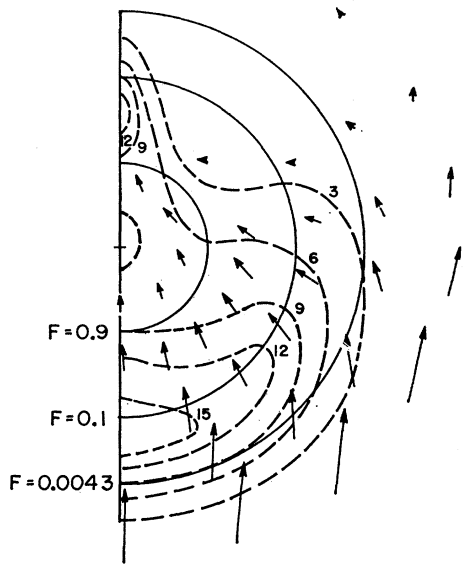


FIG. 16. The flux of 18-MeV alpha particles in the Ar nucleus.

out that completely antisymmetrized shell-model wave functions without configuration mixing are equivalent, of course, to an alpha-particle-like configuration⁴ but, of course, also equivalent to a deuteron-like configuration, etc., since antisymmetrization removes any differences between these configurations. The experiment is significant because it shows the width for the alpha-particle-cluster configuration is very large.

B. The Heavy Elements Pb, U, and Bi

In order to obtain some understanding of the magnitude (approx 0.4) of the ratio $(d\sigma/d\Omega)/(d\sigma/d\Omega)_{H_0}$ for heavy elements, a knowledge of the mean free path of alpha particles is useful. Accurate values for reaction cross sections at 40 MeV for alpha particles on a series

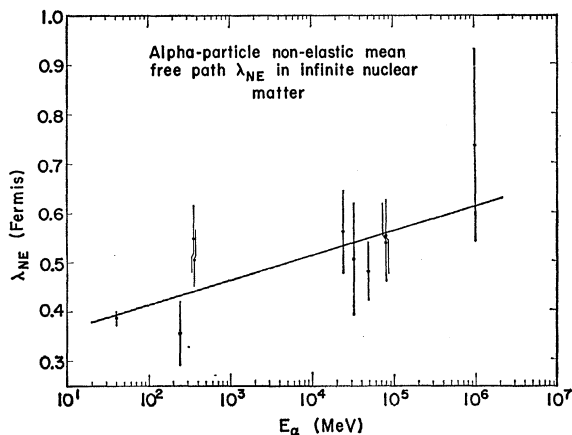


FIG. 17. The mean free path λ_{NE} in the energy range 10^1 – 10^6 vs the energy in nuclear matter of one-twentieth central nuclear density, $\rho_0/20$.

of elements¹⁵ have been measured, and a series of less accurate measurements have been made in the energy interval 10^2 – 10^6 MeV by a number of authors.^{16–18} The reaction cross section obtained from these measurements may be described in terms of a radius parameter r_0 where the reaction cross section is taken equal to $\pi r_0^2 A^{2/3}$ where suitable averaging is made on A , the atomic number, when necessary for the emulsion measurements. It is found that over the energy range 10^1 – 10^6 MeV, the reaction cross section varies only by 50% and, therefore, the nonelastic mean free path λ_{NE} of alpha particles in nuclear matter of one-twentieth density $\rho_0/20$ (equal to the density ρ of the outer surface of the nuclear matter distribution) must be similar.

An extensive analysis of the elastic scattering of alpha particles (see Fig. 15) in the 10–50 MeV range of a series of elements showed that the scattering could be characterized in terms of an optical-model potential.¹⁹ McCarthy²⁰ calculated the flux for 18-MeV alpha particles through such a potential (see Fig. 16). Since this

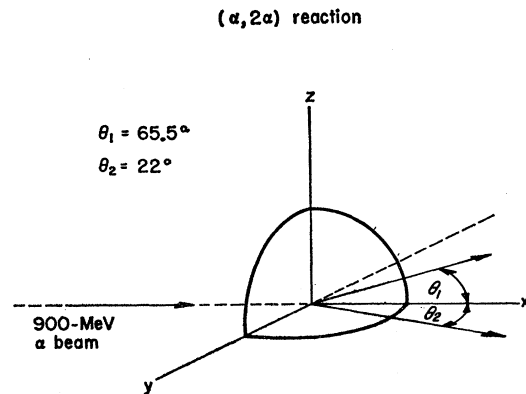


FIG. 18. A schematic diagram of the $(\alpha, 2\alpha)$ reaction.

potential in the surface region is well defined, the flux attenuation in that region will be well defined and not subject to the usual ambiguities associated with optical-model calculations. Consequently, it is possible to integrate through the nucleon density $\rho(r)$ to where the flux attenuation reaches a $1/e$ value and consequently to obtain λ_{NE} . The resulting value of λ_{NE} in the energy range 10^1 – 10^6 MeV is plotted in Fig. 17. A straight-line best fit to the experimental points is also shown.

Using the straight-line fit to the data, values of λ_{NE} in nucleon matter density $\rho_0/20$ were obtained for elastic

¹⁵ G. Igo and B. D. Wilkins (to be published).

¹⁶ G. P. Milburn, W. Birnbaum, W. E. Crandall, and L. Schechter, Phys. Rev. **95**, 1268 (1954).

¹⁷ E. Lohrmann and M. W. Teucher, Phys. Rev. **115**, 636 (1959).

¹⁸ E. Lohrmann, M. W. Teucher, and M. Schein (unpublished).

¹⁹ G. Igo, Phys. Rev. Letters **1**, 72 (1958); Phys. Rev. **115**, 1665 (1959).

²⁰ I. McCarthy, in *Proceedings of the International Conference on the Nuclear Optical Model*, Florida State University Studies No. 32 (The Florida State University Press, Tallahassee, Florida, 1959).

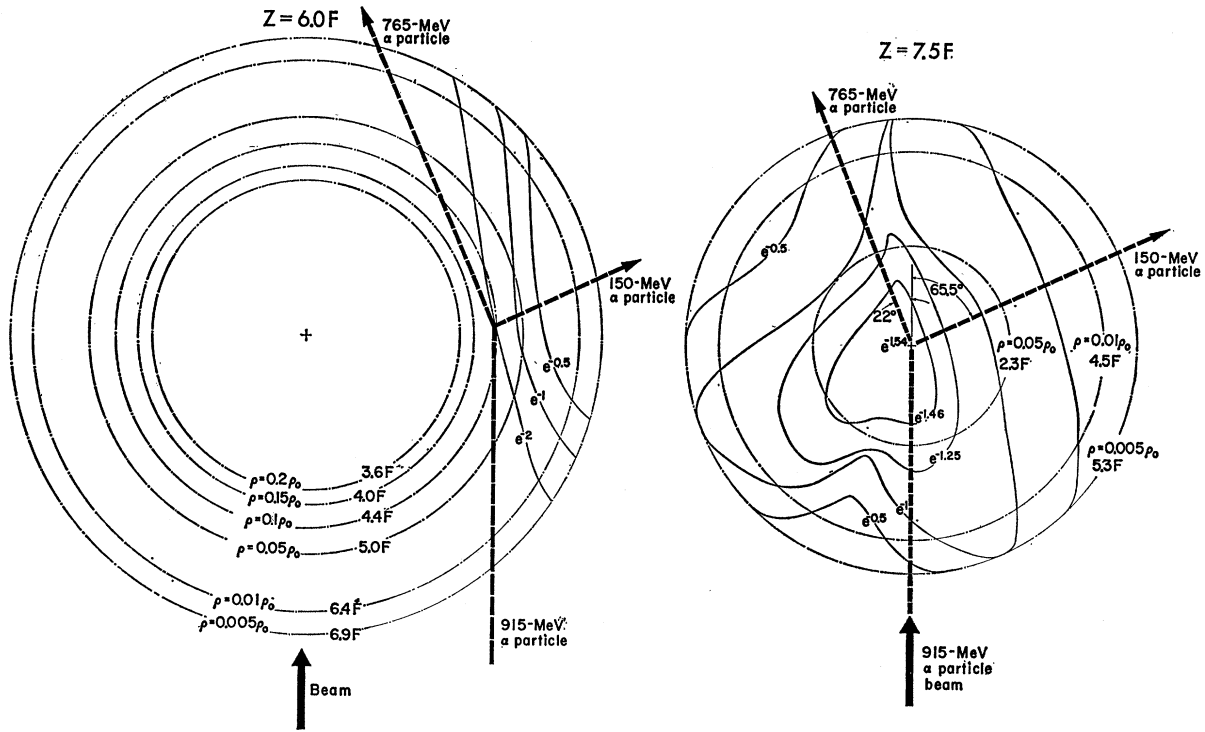


FIG. 19. Contour plots for the nuclear density $\rho(r,z)$ and the attenuation $A(r,z)$ for $(\alpha,2\alpha)$ events at 0.91 BeV.

scattering of alpha particles to $\theta_2 = 22^\circ$, $\theta_1 = 65.5^\circ$. These are 9.2 F for the incident 0.9-BeV alpha particle, 9.0 F for the 0.76-BeV alpha particle scattered to $\theta_2 = 22^\circ$, and 8.4 F for the 0.15 BeV alpha particle at $\theta_1 = 65.5^\circ$.

Since the alpha particles at these energies are not effected by the refractive effects of the Coulomb field and of the nuclear potential, and because the wavelengths associated with the momentum transfer in the collision are very small, the alpha-particle trajectories are semiclassical. They have been approximated by ray diagrams in a WKB calculation in which the attenuation is treated semiclassically and is described below.

In Fig. 18, the 0.91-BeV beam is incident along the x axis of the nucleus, the scattering event occurs in the x - y plane. The attenuation of the $(\alpha,2\alpha)$ events due to the small value of λ_{NE} was calculated at various values of z . It was found that the attenuation was so severe that almost all events were produced in the pole caps, $z \geq 7.5$ F, where $\rho \leq (1/20)\rho_0$. The results of this calculation are shown for two typical z values, $z = 6.0$ F and $z = 7.5$ F of the lead nucleus in Fig. 19. Broken circular contour lines show ρ values, and the solid contour lines show the attenuation factor $A(r,z)$ that results from the attenuation of the incident alpha-particle beam and the attenuation of the scattered alpha particles along their $\theta_1 = 22^\circ$ and 65.5° ray paths. Each of the contour paths is marked with the associated attenuation of $(\alpha,2\alpha)$ events.

Figure 20 shows the quantity

$$\phi(z) \equiv \int_0^\infty \int_0^\infty A(r,z) \rho(r,z) dx dy,$$

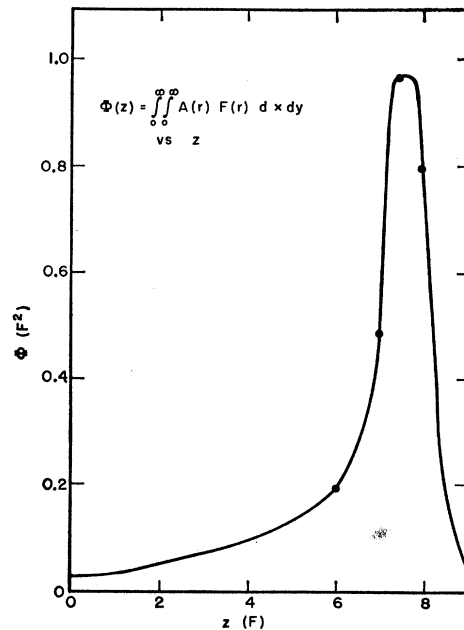


FIG. 20. The quantity $\phi(z)$ versus z . This quantity $\phi(z)$ is defined in the text.

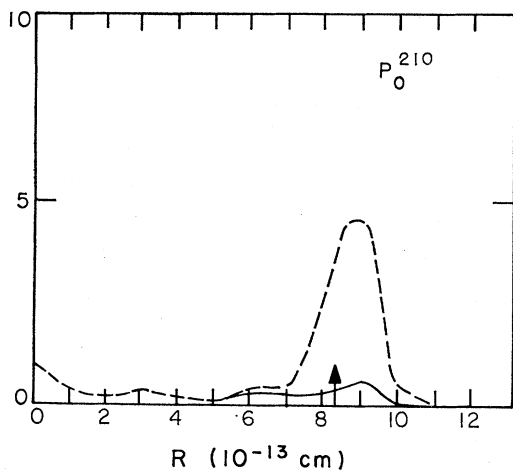


FIG. 21. The probability of alpha-cluster formation from the shell model (solid line) and the probability of alpha-cluster formation from the shell model with configuration mixing (reference 21). The arrow indicates the radius where the $(\alpha, 2\alpha)$ reaction occurs with the highest probability.

where $\rho(r, z)$ is the nuclear density at height z . The pole caps at $z = \pm 7.5 F$ contribute the most. The equivalent, nonabsorptive volume contributing as obtained from this WKB calculation is equal to $78 \pm 18 F^3$ of density $\rho_0/20$. In this volume there are $n = 4 \times (0.27 \pm 0.06)$ nucleons or 0.27 ± 0.06 "alpha-particle" clusters if clustering is complete. The measured quantity $(d\sigma/d\Omega)/(d\sigma/d\Omega)_{He}$ is 0.45 ± 0.20 . The error on the former quantity comes mainly from the straight-line approximation for λ_{NE} (see Fig. 17 and Table IV). If a line is instead drawn through the measured values of λ_{NE} , a decrease of the order of the first source of error listed in Table IV occurs in $\phi(z)$. Harada²¹ has shown that α -particle clustering occurs just in the region of high sensitivity $\rho = 0.05\rho_0$ from a shell-model calculation with configuration mixing, i.e., clustering (see Fig. 21). As mentioned in Sec. I, there is considerable amount of evidence of other kinds that suggest alpha-particle clustering exists. Ostroumov and Filov⁵ have bombarded emulsion nuclei with high-energy protons and observe alpha particles emitted which are attributed to collisions between the cascade nucleons produced by the primary and the "alpha-particle" cluster. A Monte Carlo calculation is used to follow the development of the cascade and the subsequent collision with a cluster. The results at various incident energies are consistent with this description of the process. Since the process occurs through the intermediary of a cascade product, it will be insensitive to the particulars of the last stages of the interaction where the alpha particles are produced. For instance, the alpha particles may be due to a *pick-up reaction* by a cascade proton or deuteron. The (p, α) reaction was also investigated in the few tens of MeV region by Hodgson.⁶ The same comments apply here but

²¹ K. Harada, Prog. Theoret. Phys. (Kyoto) **27**, 430 (1962).

the process is complicated by the strong refractive effects of the nuclear potential at these energies.

Another kind of evidence which indicates "alpha-particle" clustering may be occurring comes from α -decay studies.^{1-3, 22, 23} The relative values of reduced widths for alpha-particle decay have been considered by Mang for spherical nuclei²² and Mang and Rasmussen for spheroidal nuclei.²³ Rasmussen¹ has calculated absolute widths values for alpha decay using the real part of the Igo potential.¹⁹ Harada² has considered the additional effect of the imaginary potential. The general conclusion is that the ratio of reduced widths agrees well with the shell-model predictions but that the absolute magnitude are too small by a factor of about 10^{-3} .

Another source of evidence for clustering in the outer fringes of the nucleus comes from the production of Σ^- stars in emulsion nuclei by stopped K^- mesons.⁴ Figure 22 shows the region of the nucleus sampled by the K^- mesons according to a calculation by Wilkinson and his collaborators⁴ and in the $(\alpha, 2\alpha)$ experiment for comparison. Note that the $(\alpha, 2\alpha)$ reaction is sampling a less dense portion of the nuclear surface.

It should be noted that there is a limitation to the kind of information obtainable from a study of the K^- reaction. The absorption process is not sensitive to "alpha-particle" clusters specifically. It is sensitive to the presence of spatially correlated nucleons. A two-nucleon structure for example, might be involved, instead of an "alpha-particle" cluster.

The correlation experiment at 0.91 BeV, the $(\alpha, 2\alpha)$ reaction, gives evidence about the specific problem of "alpha-particle" clustering in the nuclear surface. In contrast to the (p, α) reaction, the $(\alpha, 2\alpha)$ reaction mechanism may be used virtually to exclude the possibility that the reaction proceeds as a pick-up reaction.

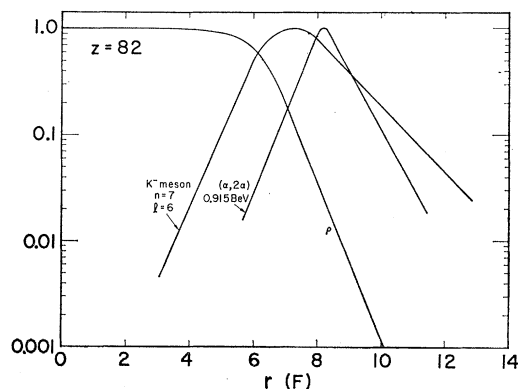


FIG. 22. The probability of absorption of K^- mesons and the nuclear form factor for bismuth, and the probability for the $(\alpha, 2\alpha)$ reaction at 0.91 BeV in lead.

²² H. J. Mang, Phys. Rev. **119**, 1069 (1960).

²³ H. J. Mang and J. C. Rasmussen, in *Proceedings of Rutherford Jubilee International Conference, 1961*, edited by J. E. Birks (Heywood and Company, Ltd., Manchester, 1962), p. 359.

The reasons for this are that (1) Both emerging alpha particles are observed rather than just one product; (2) All the energy of the incident alpha particle is carried off by the two reaction alpha particles; (3) The alpha come off preferentially at the kinematical separation angle of 87.5° ; and (4) Each alpha particle has the correct energy, namely, the kinematical energy corresponding to two-body collisions of equal mass particles.

It is, of course, possible that the incident alpha could strike a moving nucleon in the nucleus and transfer the proper amount of energy and, that, when the proton came out, it picked up a triton (or three nucleons) and the necessary momentum to appear with 180 MeV and

leave the residual nucleus nearly at rest. In order for this to happen, however, the proton would have to have a momentum very different from the expected momentum distribution.

ACKNOWLEDGMENTS

The authors wish to acknowledge the assistance of M. Brown, who designed and maintained the electronics, Q. A. Kerns and R. Tusting, for the spread-out beam system and the Ar-2 light flasher assemblies, and to J. Vale and the 184-in. synchrocyclotron crew for steady, useful ion beams.

The Energy Levels of Pd^{106} Populated in the Decays of Ag^{106} and $\text{Rh}^{106}\dagger$

W. G. SMITH*

Physics Department, Purdue University, Lafayette, Indiana

(Received 25 February 1963)

The conversion electrons of 5 high-energy transitions in the decay of Ag^{106} have been observed in a permanent magnet spectrograph. The following transitions (in MeV) were observed: the relative intensities of the K -conversion electron lines are given in parentheses: 1.0461(40), 1.1298(19), 1.2010(15), 1.2237(5), and 1.5285(12). These transitions can be fitted into a Pd^{106} level scheme, with slight modifications, proposed by Smith. This scheme was based on gamma-ray and low-energy conversion electron studies. The modified Pd^{106} level diagram is compared with the predictions of several nuclear models.

INTRODUCTION

THE study of the energy levels of ${}_{46}\text{Pd}^{106}$ populated by the electron capture decay of ${}_{47}\text{Ag}^{106}$ and by the negatron emission of ${}_{45}\text{Rh}^{106}$ has been reported in three recent publications. Robinson, McGowan, and Smith¹ made measurements of the gamma rays (singles spectra, coincidences, and angular correlations) emitted by Ag^{106} and Rh^{106} . Schemes of the energy levels of Pd^{106} populated by these two decays were presented. Smith² studied the low-energy (less than 0.935 MeV) conversion electrons of these two isotopes. Only two transitions were observed in the Rh^{106} decay and that level sequence was not changed. The Pd^{106} level scheme deduced from the Ag^{106} decay data was revised slightly from the one given in reference 1. The revised level diagram is shown in Fig. 1. AMBIYE and others³ reported on the results of gamma-ray coincidence, beta-spectrum, and beta-gamma ray coincidence measurements on Rh^{106} . This work corroborated the level scheme of Robinson *et al.*¹; spin and parity assignments for the two highest lying levels were suggested. The existence of the (4+) level

at 1.23 MeV shown in Fig. 1 was verified by the excitation with 45-MeV oxygen ions of this state by Eccleshall *et al.*⁴

The observation of the conversion electrons of the high-energy transitions in the decay of Ag^{106} is presently reported. These results generally confirm the level scheme presented in reference 2. It was necessary to change only the higher lying levels of Pd^{106} . The levels at 2.7336 and 2.3636 or 1.9469 MeV were removed and levels at 2.7384 and 2.0771 MeV were added.

EXPERIMENTAL PROCEDURE AND RESULTS

The Ag^{106} production and separation has been described previously.⁵ The conversion electron lines were observed in a permanent magnet spectrograph with a field of 520 G. Intensity measurements were made with a photodensitometer and chart recorder. The relative energy measurement errors are estimated to be $\sim 0.05\%$; the absolute energy errors are estimated to be $\sim 0.1\%$. The intensity errors of the strong lines are probably $\sim 15\%$ and for the weak lines $\sim 25\%$.

The present experimental results are given in Table I, together with the results of Alburger and Toppel.⁶

[†] Work supported in part by the U. S. Atomic Energy Commission.

* Deceased.

¹ R. L. Robinson, F. K. McGowan, and W. G. Smith, *Phys. Rev.* **119**, 1692 (1960).

² W. G. Smith, *Phys. Rev.* **122**, 1600 (1961).

³ S. Y. Ambiyé and R. P. Sharma, *Nucl. Phys.* **29**, 657 (1962).

⁴ D. Eccleshall, B. M. Hinds, M. J. L. Yates, and N. Macdonald, *Nucl. Phys.* **37**, 377 (1962).

⁵ W. G. Smith, *J. Inorg. Nucl. Chem.* **17**, 382 (1961).

⁶ D. E. Alburger and B. J. Toppel, *Phys. Rev.* **100**, 1357 (1955).